J. Electrochem. Sci. Eng. **11(3)** (2021) 179-195; http://dx.doi.org/10.5599/jese.1014

Open Access : : ISSN 1847-9286

www.jESE-online.org

Original scientific paper

Molecular interaction of natural dye based on *Zea mays* and *Bixa orellana* with nanocrystalline TiO_2 in dye sensitized solar cells

Arnold Huamán[1,2], Karim Salazar[3] and María Quintana[1,✉]

[1]*Universidad Nacional de Ingeniería, Av. Tupac Amaru 210, Rímac 15333, Lima, Perú*
[2]*Universidad Tecnológica del Perú, Av. Arequipa 265, Cercado de Lima 15046, Lima, Perú*
[3]*Universidad Nacional Agraria La Molina, Av. La Molina s/n, La molina 15024, Lima, Perú*

**Corresponding author:* ✉mariavnac@yahoo.com

Received: June 4, 2021; Revised: July 13, 2021; Accepted: July 15, 2021; Published: July 21, 2021

Abstract

This work studies the interaction between natural dyes obtained from Peruvian Zea mays and Bixa orellana seeds and nanostructured titanium dioxide, in order to evaluate their function as sensitizers into solar cell devices. The effective attachment of dyes to the TiO_2 layer is corroborated by the comparison of UV-Visible absorption and FT-IR spectra of the extracted dye solutions and sensitized TiO_2 electrodes. The principal compounds from the seed extraction of Zea mays and Bixa orellana are cyanidin-3-glucoside (C3G) and bixin respectively, which were analyzed in an isolated dye/cluster TiO_2 system by molecular dynamic simulation. The results showed that chemisorption is carried out through a consecutive deprotonation process, and Ti-O bond formation by the monodentate OH and COOH anchoring groups, for C3G and bixin respectively. Finally, we tested the effect of the dye - TiO_2 interaction on the charge transfer by the comparison of the current-voltage curves and incident photon-to-current conversion efficiency (IPCE) of the cells. We found that dye agglomeration in films with Bixa orellana and high charge recombination of films with Zea mays are critical points to be solved. For this reason, we propose the pretreatment of the TiO_2 film before sensitization with Bixa orellana and analyze the effects of pH in Zea mays solution, in order to obtain better device efficiencies.

Keywords

Molecular dynamic simulation; nanostructured titanium dioxide; plant colorants; sensitizer chemisorption.

Introduction

The third-generation of photovoltaic cells employs mainly organic molecules nanocrystalline materials. The high band gap semiconductor compound TiO_2 is extended to the visible spectrum

absorption by the addition of dyes (known as sensitizers). The dye-sensitized solar cells (DSSC) are solar energy conversion devices that since their appearance, have attracted considerable attention due to their low production cost and the environmental friendliness. This type of solar cell bases its operation on the regeneration of dye molecules by a redox system based from electrolyte, which is regenerated by the coming electrons from an external load [1]. The heart of the system consists of a mesoporous oxide layer composed by nanometric particles attached with dye molecules, which are responsible for activating the charge transfer. The sensitizing dye plays a very important role in the process of solar conversion into electrical energy. Numerous metal and organic complexes have been synthesized as sensitizers, the most efficient being those based on the ruthenium complexes [2,3]. However, from the environmental point of view, the presence of this heavy metal in synthesized dyes is undesirable and besides, the methods of their preparation are still complicated and expensive. In this sense, the dyes obtained from natural dyes appear to be good alternatives due to their non-toxicity, low-cost production and complete biodegradation.

Natural dyes, including plant colorants such as anthocyanins [4-12], betalains [13-16], chlorophyll [17-21] and carotenoids [22-24], have already been targeted in many studies. For this particular work, two natural products from Peru have been used. The first is *Zea mays*, known as purple maize. This product is rich in anthocyanins, which give it the characteristic purple color. The main compound of the group of anthocyanins is cyanidin-3-glucoside (C3G) and, to a lesser extent, pelargonidin-3-glucoside, peonidin-3-glucoside and cyanidin-3-(6"-malonylglucoside) [25]. The second is *Bixa orellana*, also called Achiote. It is a tropical shrub native to the southwestern Amazon, which has an inedible red fruit with about 50 seeds. A dark red extract is obtained from Achiote seeds, which is widely used as coloring and flavoring. The pericarp of seeds contains a high concentration of carotenoids, which make up to 80 % of the carotenoid 9'-cis-bixin or bixin. The remaining 20 % includes trans- and cis-norbixin [26]. The chemical structures of the main components of these dyes are shown in Figure 1.

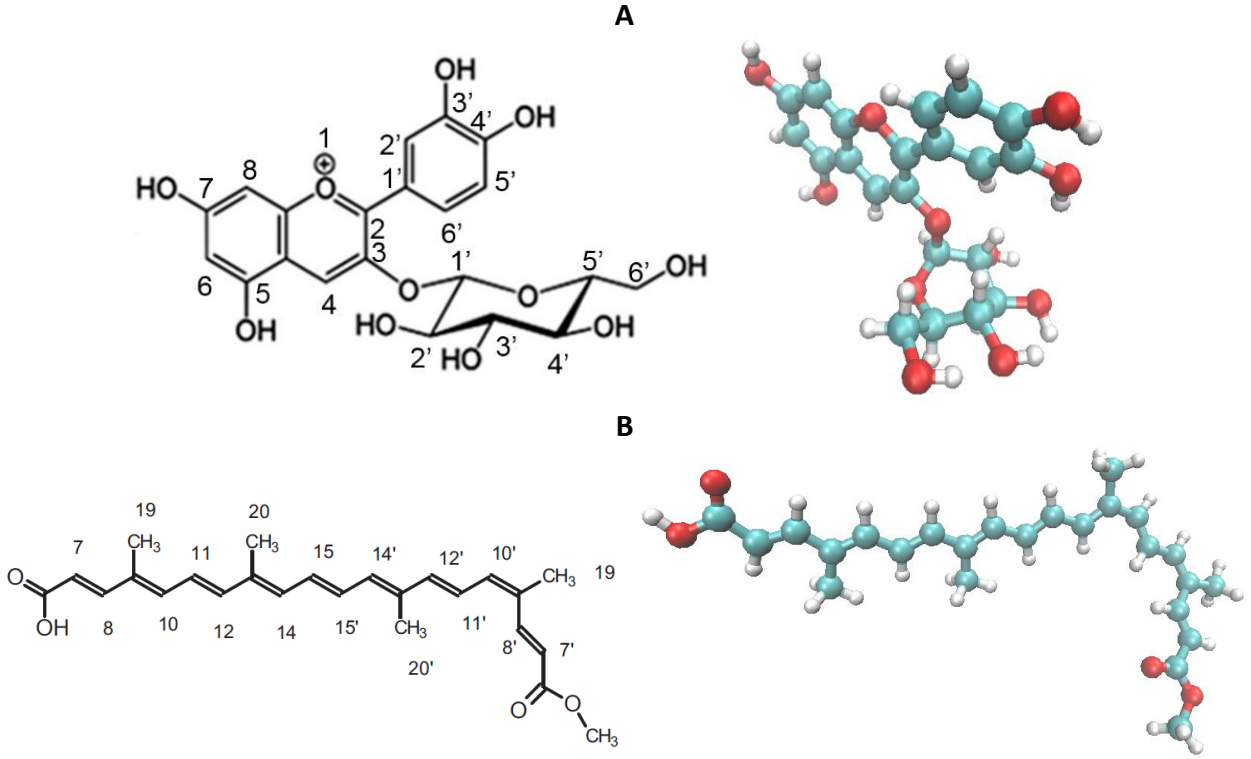

Figure 1. *Chemical structure and optimized geometry of cyanidin-3-glucoside (A) and apocarotenoids cis-bixin (B)*

Commonly, natural sensitizers present lower efficiency due to their limited light absorption capability and weak bonding with semi-conductor network [27]. For this reason, it is necessary to understand the interaction of the plant-based dye with TiO_2 cluster in order to develop more efficient materials to improve the efficiency of natural DSSCs (Figure 2).

In this article we analyze the sensitization mechanism of natural dyes obtained from *Zea mays* and *Bixa orellana*. A combined theoretical and experimental study is carried out to achieve this purpose. The interaction between the main components of both dyes with a TiO_2 cluster is analyzed using molecular dynamics simulation (MDS). FTIR and UV/Vis spectroscopy methods, in addition to verifying the sensitization and identifying the functional anchoring groups of the dyes, provide an experimental corroboration of the theoretical mechanisms proposed by MDS. The most favorable characteristics for the sensitization of each particular dye revealed by this study, allow us to propose additional procedures for the optimization of dye preparation.

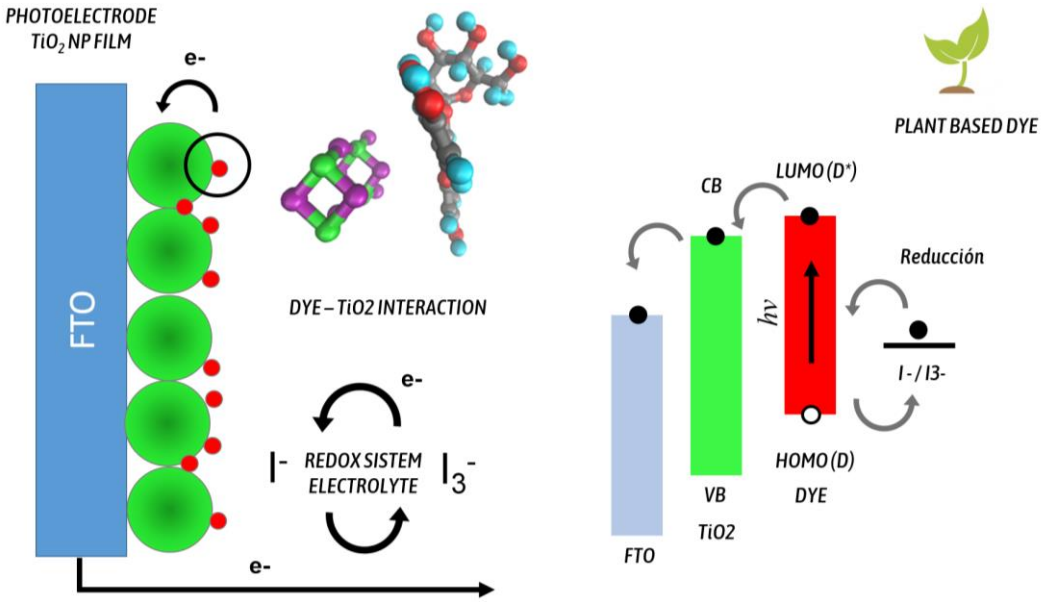

***Figure 2**. Architecture of dye-sensitized solar cell from this study*

Experimental

Extraction of natural dyes

The purple corn was first unshelled and dehydrated at 80 °C overnight. Then the crown of the corn was scratched to obtain floccules from the surface layer, which were crushed with a mortar to obtain a fine powder. The obtained product was diluted in water in 1:500 ratio by weight. After one hour of heating at 80 °C, the solution was filtered and centrifuged at 3000 rpm by 30 min. The powder obtained from achiote seeds was diluted in acetone in 1:100 ratio by weight. After one hour of vigorous agitation, the solution was filtered. The concentration of anthocyanins contained in the purple corn solution was calculated with the method of Wrolstad *et.al*. [28], obtaining 14.65 µM. The concentration of bixin contained in the achiote solution was approximately 0.26 µM, and was calculated using Lambert's law [29].

Preparation of solar cells sensitized with dye

Glasses coated with fluorine-doped tin dioxide (FTO) with sheet resistance of 15 Ω/sq (1.1 mm) were used, which were previously washed and rinsed in an ethanolic solution of 0.1 M HCl. A paste of titanium dioxide nanoparticles DSL 30NR-D provided by the Solaronix company was deposited on

the conductive substrate using doctor-blade (tape casting) method in a circular area delimited by 3 mm radius. The film was consolidated by a heat treatment at 450 °C for 45 min. Figure 3 shows SEM images of one of the films prepared with this method. Films were made up of particles whose sizes range from approximately 20 to 50 nm. The average thickness of the films was 8 µm.

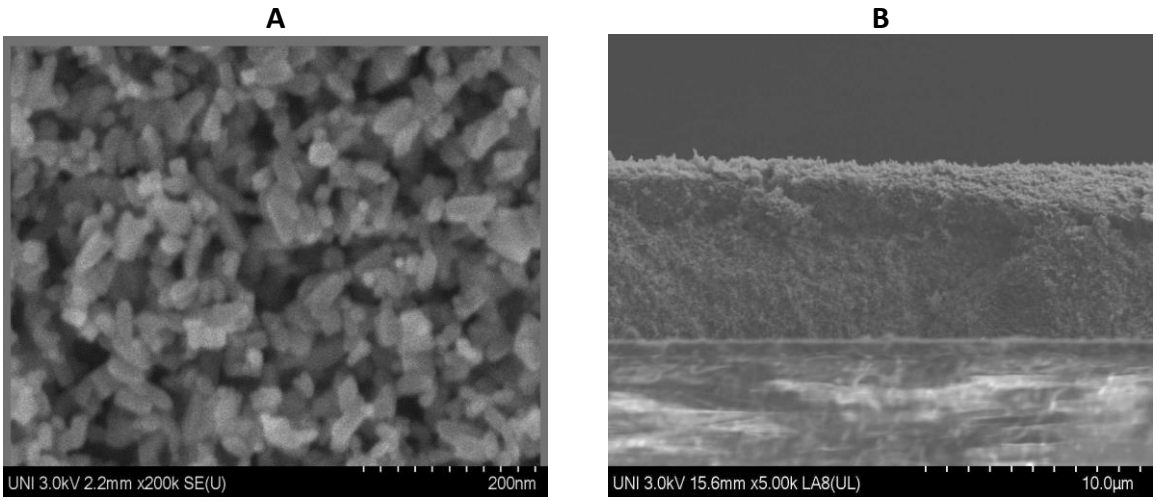

Figure 3. *SEM images of the front (A) and side (B) view of TiO_2 film prepared with doctor blade method*

The experimental XRD pattern in Figure 4 agrees with the JCPDS card Nº 21-1272 corresponding to anatase TiO_2, while the other peaks correspond to the FTO film. The electrodes were immersed in the corresponding solutions containing the natural colorant in a period of 18 hours. On the other hand, a chloroplatinic acid solution was prepared to obtain platinum films by heat treatment at 450 °C for 15 min. The solar cells were assembled into redox electrolyte, constituted by tetra-n-butylamonium iodide (TBAI) 0.6 M and 0.05 M iodine (I_2) in acetonitrile [30] put between the sensitized conductive glass/FTO electrode and the platinum counter electrode.

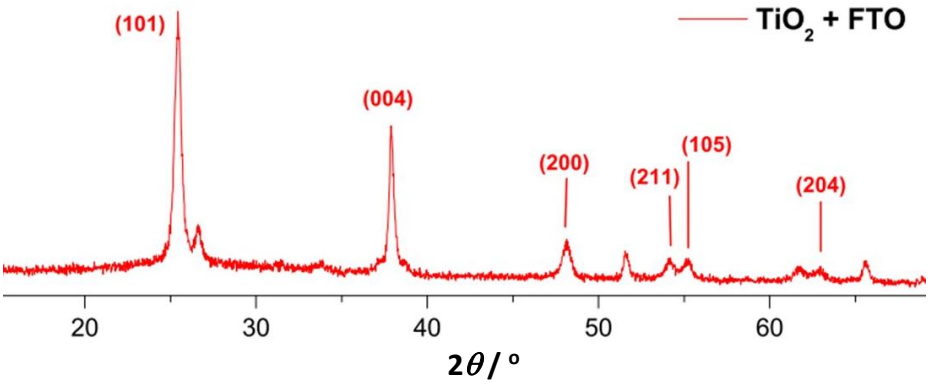

Figure 4. *XRD pattern of TiO_2 film on FTO prepared with doctor blade method*

Characterization

Natural colorants solutions and sensitized TiO_2 films were characterized using UV-Visible USB4000 spectrophotometer from Ocean Optics. The Fourier-transform infrared (FTIR) spectra were obtained by a Nicolet iS10 team from Thermo Fisher. The Current-Voltage curves of the solar cells were tested under a standard light source, which consists from a white light emitting diode (LED). The light intensity was 1 sun equivalent (1000 W m^{-2} AM1.5G). Incident photon-to-current conversion efficiency (IPCE) was measured by an IPCE station consisting mainly of 175 W Xenon lamp source, Monochromator CM110 (Spectral Products), Si calibrated detector and a digital acquisition board Labjack U6.

Computational methods

Molecular dynamics simulations of the complexes TiO_2 and isolated dyes were carried out with an initial separation of 5.0 Å between them. The TiO_2 cluster corresponds to anatase configuration and consists of two-unit cells, resulting in a small cluster of 12 atoms. The initial structures of the complexes were equilibrated during 8 ns simulation time, while the individual component was equilibrated during 4 ns. The force field used is Reax FF for all the molecular dynamics simulations [31]. It allows the study of reactive environments, and its algorithms is based on the bond order calculations. During the calculation, the charge equilibration is performed in all the molecular system. The used ensemble is NVT at 300 K, which allows to maintain the system at the constant temperature at environmental condition with mass conservancy. The energy of the molecular system is calculated solving the potential and kinetic energy. The calculation of the binding energy of the dye/TiO_2 complex is performed by the following operation, the total energy of the complex minus the total energy of each componen., taking into consideration the average of the total energy of the molecular system each 1000 fs.

Results

FTIR characterization of natural dyes

The FT-IR spectra of natural dyes can provide information about the functional groups from the plant extraction compounds, which allows the identification of the most abundant dyes from each extraction and its interaction with TiO_2 NP film. That is why we compare the measurements taken on dye samples before and after the sensitization.

The IR analysis of the *Zea mays* extraction in powder is shown in Figure 5A. It has common vibration band of functional groups present in cyanidin-3-glucoside (C3G) dye such as OH functional groups (3271 cm^{-1}), C-H stretching vibrations modes of benzenic ring (2915 cm^{-1}), carbonyl group (1718 cm^{-1}), C=C aromatic ring stretching vibrations (1604 cm^{-1}), and ester linkage (1048 cm^{-1}) [32]. The detected functional groups confirm the presence of anthocyanins in the *Zea mays* (ZM) sample, which is correlated to the cyanidin-3-glucoside (C3G) structure.

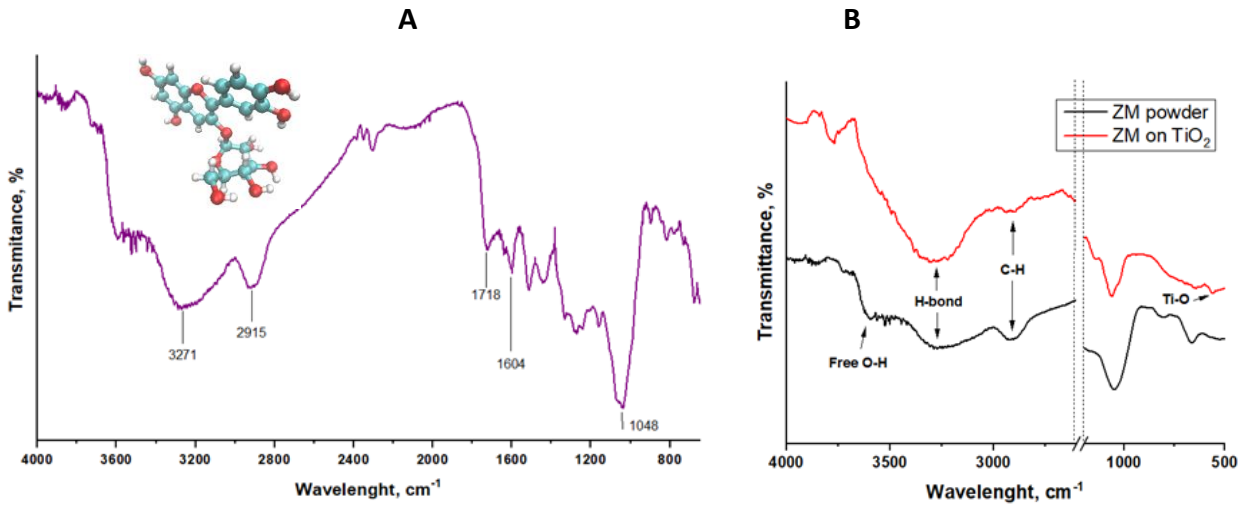

Figure 5. *FT-IR spectrum of dye present of Zea mays extraction in powder (A) and its comparison with FT-IR spectrum of dye on TiO_2 (B)*

After sensitization onto TiO_2, we observe in Figure 5B that the peak corresponding to free OH bonds (3600 cm^{-1}) in the powder sample [33] disappear, passing to form a single band corresponding to -H bonds that include inter and intramolecular interactions [34]. Another interesting peak

corresponds to the C-H stretching from benzene, which becomes weak and shift to the red (2910 cm^{-1}) after sensibilization. These chemical bond vibrations could be affected by the interaction between the molecules themselves or with the TiO_2 cluster. However, the most effective evidence of chemical interaction between the dye and the electrode is the presence of Ti-O at 559 cm^{-1} [35].

FT-IR spectra of dried *Bixa orellana* powder and the vibrational modes shown in Figure 6A suggests the presence of apocarotenoid cis-bixin (bixin) compound because of the designation of characteristic peaks: C-H stretch due to the methyl and methylene group at 2922 and 2851 cm^{-1}, carboxylic acid group at 1713 cm^{-1}, alkene C=C stretch at 1642 cm^{-1}, the asymmetric bending vibrations of the methyl -CH_3 group at 1377 cm^{-1}, stretching vibration of C-O at 1286 cm^{-1}, and the symmetric and asymmetric C-O-C ether groups at 1248 and 1151 cm^{-1} [36].

Figure 6B shows a decrease in the peak corresponding to C=O stretching of the carboxylic acid group (1713 cm^{-1}). Typically, this peak disappears after dye - electrode interaction through the carboxylic group [37]. However, this band does not disappear completely, suggesting that presence of molecules on the surface are stacked and create a shielding effect. A broadening of the band assigned to the C=C alkene bond (1642 cm^{-1}) is observed, which suggests the presence of macroaggregates [38], which would confirm the aforementioned effect. Another interesting peak corresponds to the methyl group, which is shifted to the red (from 1371 to 1365 cm^{-1}), what could be due to interaction through this group at the interface. In addition, a small peak appears after the dye sensibilization corresponding to Ti-O bond formation at 503 cm^{-1} [35].

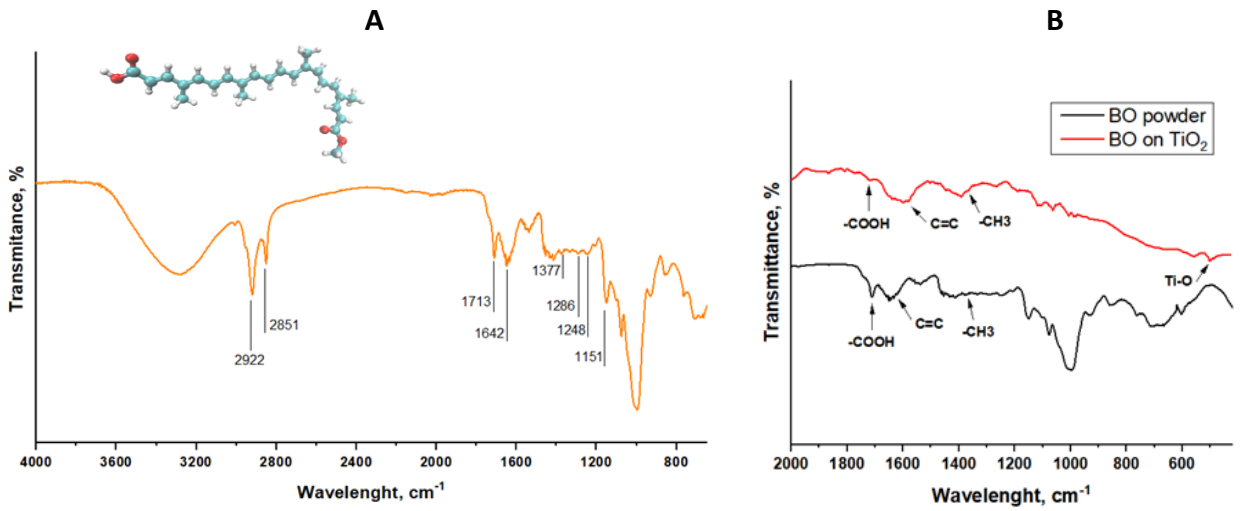

Figure 6. *FT-IR spectrum of dye present in Bixa orellana extraction in powder (A) and its comparison with FT-IR spectrum of dye on TiO_2 (B)*

UV-Visible characterization of natural dyes

In order to assure the dye/TiO_2 interaction, we run UV-Vis spectrometry for the extracted natural dyes when they are in solution and after being absorbed on TiO_2. In Figure 7, the absorption spectrum of the *Zea mays* solution shows a maximum peak at approximately 520 nm within the typical broad absorption peak of anthocyanins, which is the main compound of this dye [39]. While the absorption band of the adsorbed dye onto semiconductor film is broadened, the corresponding maximum is red shifted with respect to their solution [40]. The visible absorption band can shift to a lower energy due to the complexing with metal atoms [41]. The broadening of the absorption band is also an indication of a charge transfer interaction between the sensitizing dye and TiO_2 surface [42].

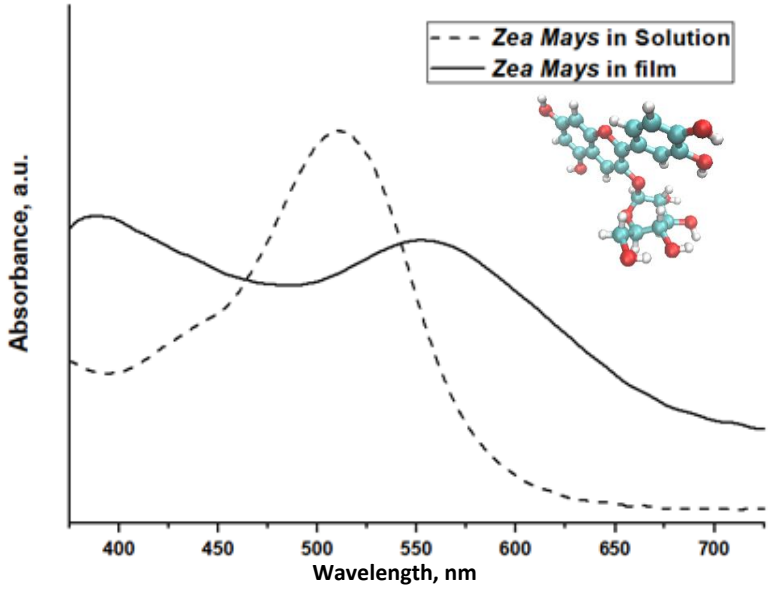

Figure 7. *UV-Visible absorption spectra of the extraction from Zea mays in water solution (dotted line) and adsorbed on TiO_2 (solid line)*

Figure 8 shows three absorption peaks for the *Bixa orellana* solution spectrum located at approximately 435, 460 and 490 nm, coinciding very well with the bixin spectrum which is the main compound within the group of carotenoids that make up this dye [43]. Once the dye is adhered on the TiO_2 surface, the absorption spectrum gets wider. In addition, the intensity of maximum absorption peaks increases, which shows the resulting strong interaction between bixin and TiO_2 surface [44]. It shows blue-shifted peaks in the spectra of bixin absorbed in TiO_2, which has been attributed to the aggregate formation of dyes and/or the disarraying of dyes on TiO_2 surface [45].

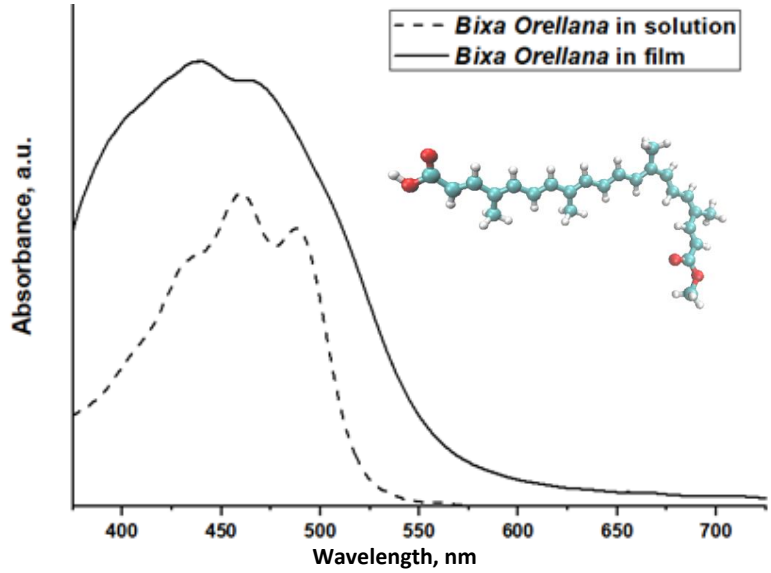

Figure 8. *UV-Visible absorption spectra of the extract from Bixa orellana in ethanol solution (dotted line) and adsorbed on TiO_2 (solid line)*

Molecular dynamic simulations of the complexes TiO_2 and isolated dyes

The carbonyl and hydroxyl groups represent the linking groups for the attachment of dye molecules to TiO_2 [46]. In order to evaluate how dye interacts with TiO_2 electrode, molecular dynamics simulations of the complexes using Reax FF were performed. We build the initial configuration of the complex dye/anatase TiO_2 cluster (n=12), considering a monomeric dye adsorbent on

cluster. In the initial complex system (Figure 9), C3G is located over the cluster by the cyanidin side at the distance of 5 Å.

In the initial complex system (Fig. 9), C3G is located over the cluster by the cyanidin side at the distance of 5 Å. Figure 9 shows the progression of the dynamic simulation of the complex TiO_2-C3G through snapshots at relevant events. It shows that the first hydrogen lost from the OH group of C2' glucoside part occurs at 5 ps, and this proton passivates TiO_2 over the surface oxygen.

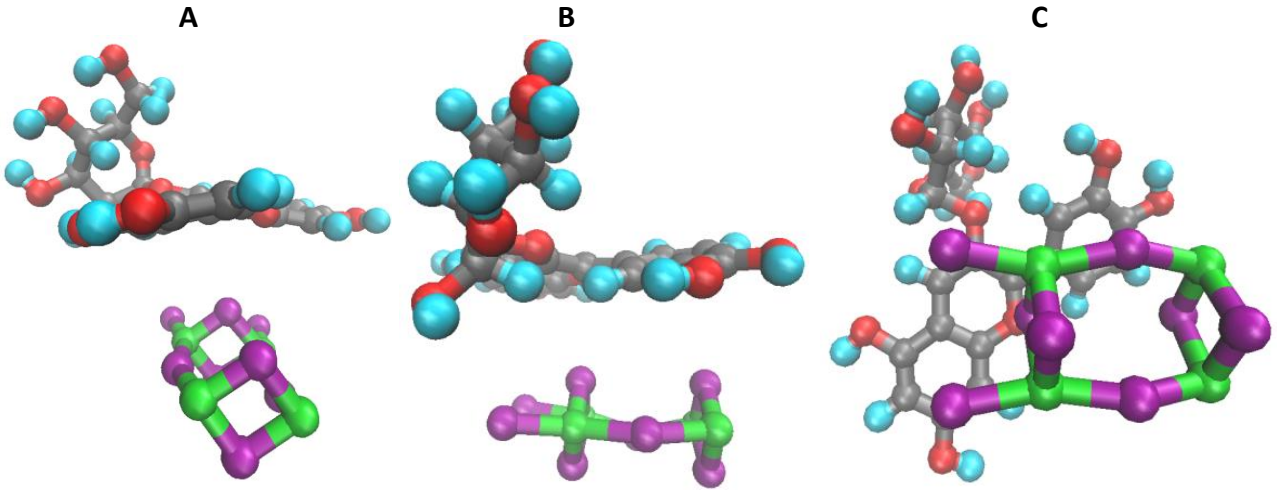

Figure 9. *Initial structure of the complex C3G/TiO_2 cluster: side view (A), back view (B) and bottom-up view (C). Color code: oxygen from TiO_2 cluster (magenta), titanium (green); oxygen from dye (red), carbon (grey) and hydrogen (cyan)*

Figure 10 shows the progression of the dynamic simulation of the complex TiO_2-C3G through snapshots at relevant events. It shows that the first hydrogen lost from the OH group of C2' glucoside part occurs at 5 ps, and this proton passivates TiO_2 over the surface oxygen. At 21 ps, an intramolecular hydrogen bond between the oxygen from OH group of C3'cyanidin and hydrogen from C2' glucoside leads the proton transfer. At 23.6 ps, the oxygen from OH at C4' of cyanidin is close to titanium atom at 1.93 Å forming a bond. At 27.5 ps, the second hydrogen from OH at C6' of the glucoside is lost and forms a part of TiO_2 surface. The hydrogen, which forms the hydrogen bond between the cyanidin and glucose, is finally transferred to the glucose side at 29 ps. At 545.5 ps, C6' of the glucoside part is close to oxygen from TiO_2 at 1.67 Å, and then at 859.5 ps, the glucoside get stability with TiO_2 by hydrogen bonds. Finally, the constant hydrogen transfer between the glucose (C2') and cyanidin (C3') is stabilized when the OH at C3' cyanidin is formed after the hydrogen lost at continues C4' at 1.8 ns. The third hydrogen lost comes from the OH at C4' glucose at 3.2 ns. At 7 ns the complex gets stabilized after the dye lost three hydrogens and forming one Ti-O and two hydrogen bonds.

Figure 11 shows the initial configuration of the complex bixin-TiO_2 cluster that maintains a separation of 5.0 Å, and the dye is located over TiO_2 by COOH side.

Figure 12 shows the progression of the dynamic simulation of TiO_2-bixin through snapshots at certain events, such as passivation process of the semiconductor with hydrogens and the formation of Ti-O bond. H bonds at 1.0 ps between hydrogen atoms at C8 and CH_3 19 with oxygen atoms from TiO_2 cluster. At 2.0 ps, a new hydrogen bond is formed between the hydrogen from COOH and the oxygen from TiO_2. A hydrogen lost from COOH occurs at 3.0 ps. At 4 ps the Ti-O bond is formed and the chemisorption between dye and TiO_2 cluster becomes stronger (1.8 Å). The second hydrogen lost occurs from the hydrogen CH_3 19 to TiO_2 cluster at 15.7 ps, and subsequently the hydrogen from the remaining CH_3 19 forms a hydrogen bond with TiO_2 at 15.8 ps.

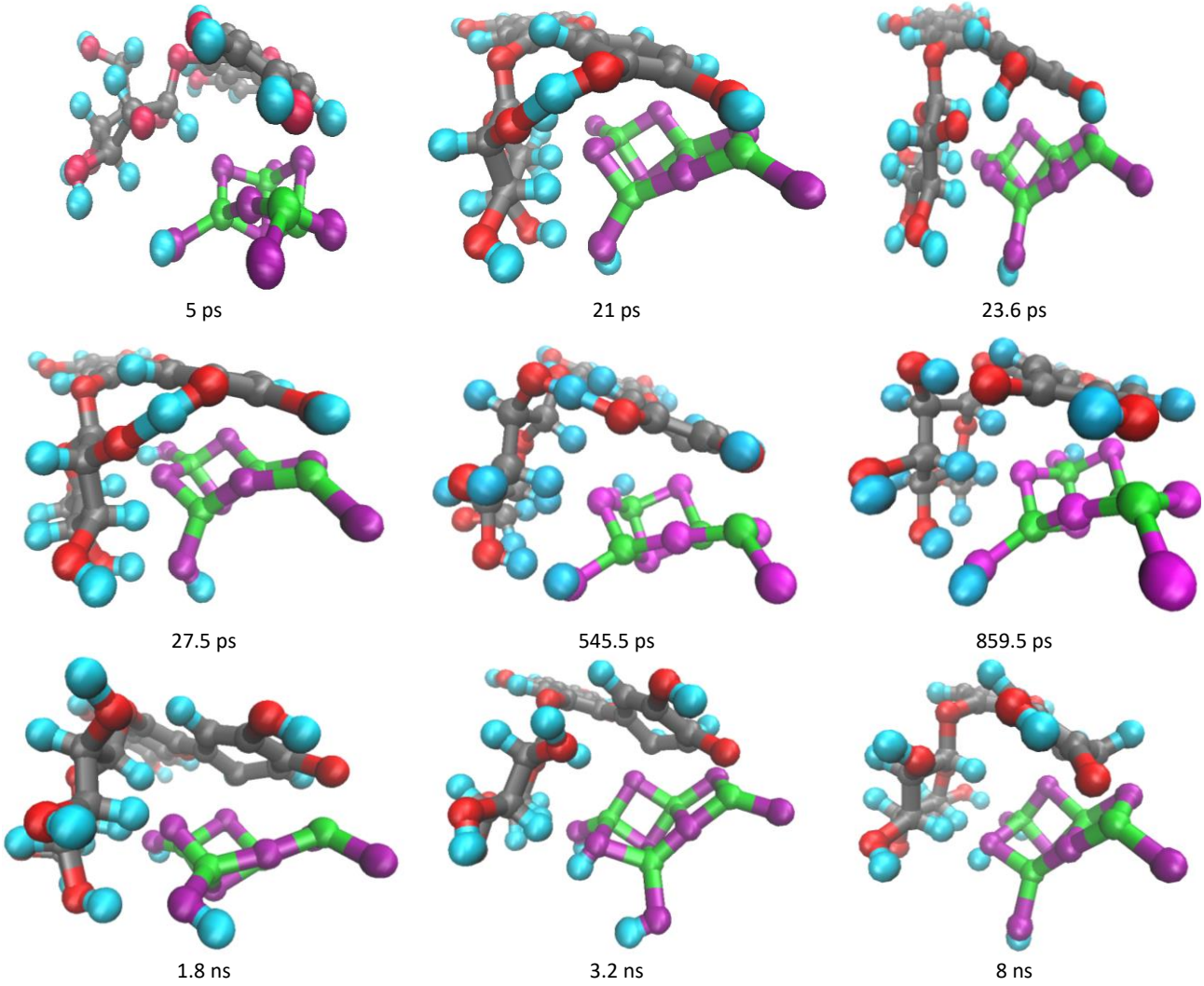

Figure 10. *Snapshots of the dynamic molecular simulation of C3G and TiO_2. Color code: oxygen from TiO_2 cluster (magenta), titanium (green); oxygen from dye (red), carbon (grey), and hydrogen (cyan)*

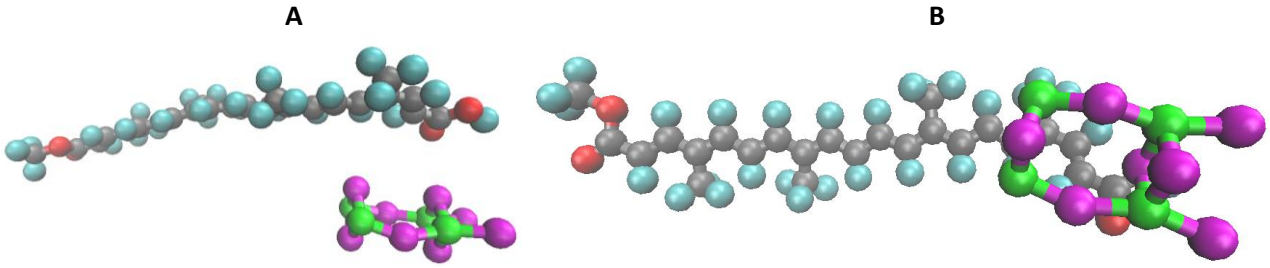

Figure 11. *Initial structure of the complex bixin/TiO_2 cluster: front view (A) and bottom-up view (B). Color code: oxygen from TiO_2 cluster (magenta), titanium (green); oxygen from dye (red), carbon (grey) and hydrogen (cyan)*

The dye migrates on the surface, and new hydrogen bond is formed between the hydrogen from CH3 20' and TiO_2 cluster at 685 ps. The hydrogen atom from C11' is lost and form a bind to the oxygen from TiO_2 at 1.918 ns, forming an alkyne at C11'. Then, the dye wraps up the TiO_2 cluster at 1.944 ns increasing the contact area between them. The self-folding of the dye molecule on TiO_2 surface occurs at 3.632 ns, and this event stabilizes bixin on the surface better.

Figure 13 shows the summary of the principal events that occurred in the dynamic simulation during 8 ns for both complexes (C3G/bixin and TiO_2). The corresponding numbering of C3G and bixin molecules are presenting in order to identify the progression of the trajectory of atoms.

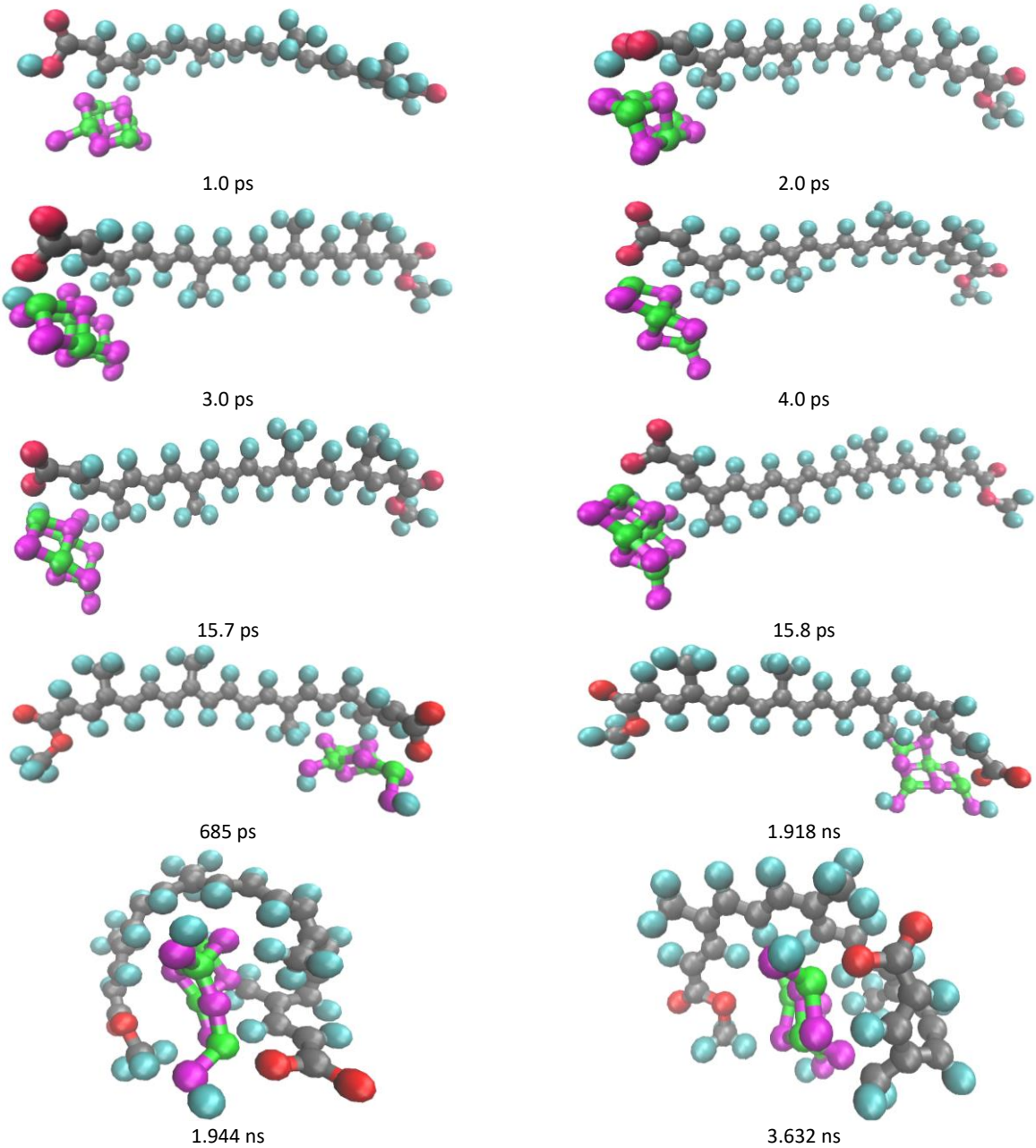

Figure 12. *Snapshots of dynamic simulation of bixin and TiO_2. Color code: from dye carbon (grey), oxygen (red) and hydrogen (cyan); from TiO_2 cluster oxygen (purple) and titanium (green)*

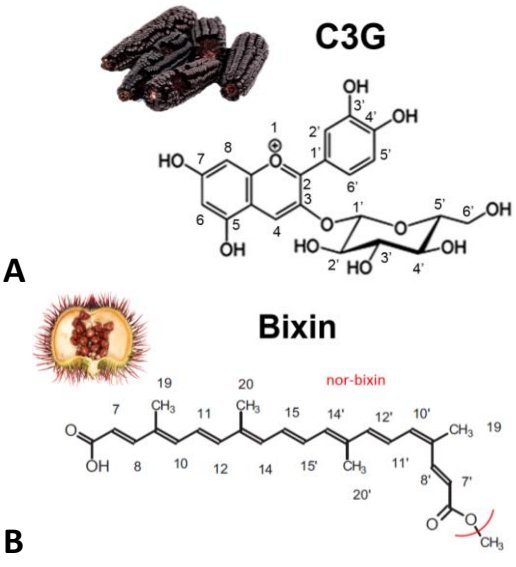

5 ps Sugar C2' – OH Hydrogen lost
21 ps Cyanidin C3'-OH • • HC2' Sugar
23.6 ps Cyanidin C4'-O – Ti (TiO_2) 1.83 Å
27.5 ps Sugar C6' – OH Hydrogen lost
545.5 ps Cyanidin C6' – O (TiO_2) 1.67 Å
859.5 ps Sugar C4'-OH • • O (TiO_2) 1.70 Å
859.5 ps Sugar C5'-H • • O (TiO_2) 1.73 Å
1.8 ns Cyanidin hydrogen transfer from OH C4' to the oxygen C3'
3.2 ns Sugar C4'-OH Hydrogen lost
1.0 ps 8CH •• O(TiO_2) and 19CH3 •• O(TiO2) 1.7 Å
2.0 ps COOH •• O(TiO_2)
3.0 ps 7'C – COOH Hydrogen lost
4.0 ps Ti-O(7'C-COO) bond 1.80 Å
15.7 ps 19CH3 Hydrogen lost
15.8 ps 19CH2 •• O(TiO_2)
685 ps 20'CH3 •• O(TiO_2)
1.918 ns 11'CH Hydrogen lost
1.944 ns dye wrap up TiO_2 cluster
3.632 ns dye self-folding on the TiO_2 Surface

Figure 13. *Numeration and summary of dynamic molecular simulation of cyaniding-3-glucoside (C3G) (A) and 9'-cis-bixin (bixin) (B)*

Binding energy of the dye/TiO_2 and dye dimer complexes

We calculate the binding energy of the dye (bixin and C3G) with a small cluster of TiO_2 in order to understand the effect of the dye/electrode interaction on the photocurrent of DSSC device. Because we suspect that there is an aggregation event during the bixin/TiO_2 interaction, which causes UV/Vis blue shift of bixin in solution compared to bixin adsorbed on TiO_2, we calculated the binding energy of both dye dimers. In order to get these results, we optimize each isolated element of the complexes. Figure 14 shows the stable configuration of the small anatase TiO_2 cluster, which occurs when all titanium atoms are 4-coordinated. It also shows that for the isolated bixin, the stable configuration is almost linear. In other words, bixin does not prefer to fold over it. Isolated C3G configuration remains almost the same in isolation and with TiO_2 interaction.

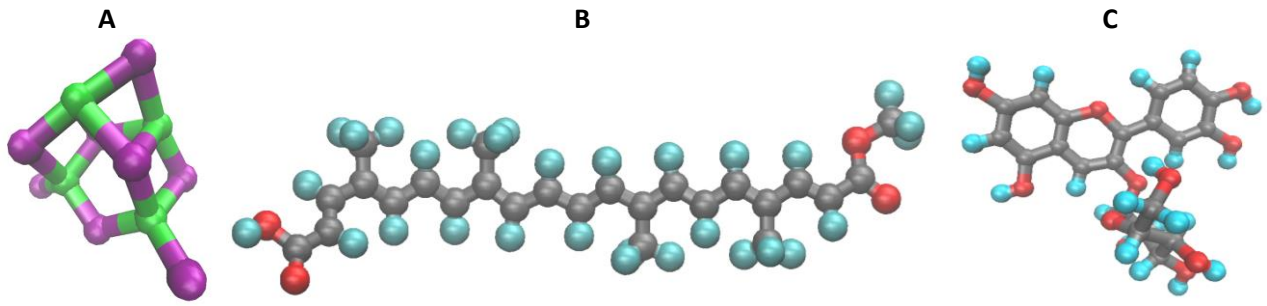

Figure 14. *Optimized n=12 TiO_2 cluster (A), bixin (B), and C3G (C) molecules*

Figure 15 shows the optimized dyes dimers after 8 ns molecular dynamics simulation at 300 K. It shows for C3G dimer that benzene rings overlap and get closer (3.5 Å), while hydrogen bonds among OH groups of the glucoside part of C3G dyes stabilize the rest of the complex. C3G dimer gets stable when the dipole moments rearrange according to the edge-to-edge. On the other hand, the bixin dimer distance between aliphatic site is 3.2 Å and the dipoles rearrange according to edge-to-face motif.

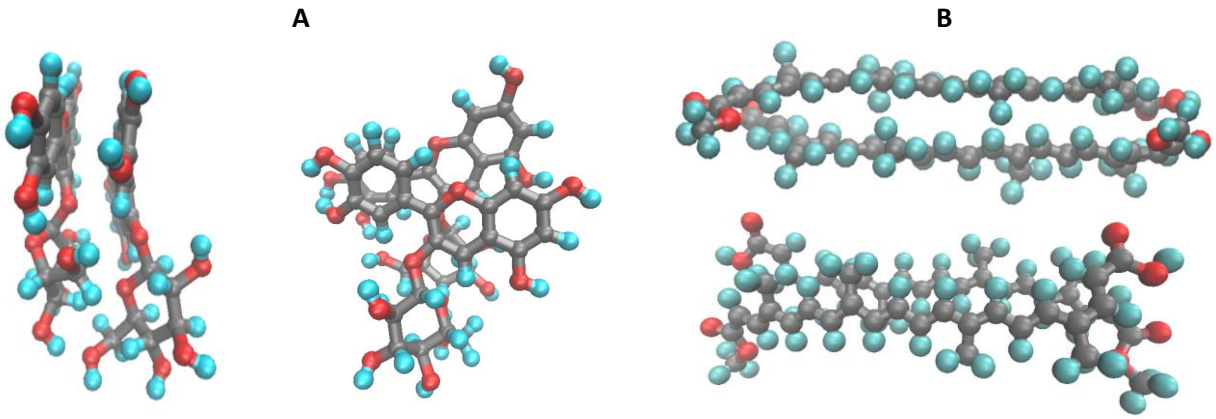

Figure 15. *Optimized structures of dye dimers: C3G (A) and bixin (B) molecules*

Table 1 shows the biding energy values of the dye to TiO_2 electrode and dye dimer. Bixin shows a better affinity to TiO_2 (-78.12 kJ mol^{-1}) than C3G. However, dyes prefer to associate by themselves (aggregation).

Table 1. *Binding energy of complexes dye/TiO2 cluster and dye dimmers*

Complexes	Binding energy, kJ mol^{-1}
C3G-TiO_2 cluster	-0.79
C3G dimer	-144.14
Bixin-TiO_2 cluster	-78.12
Bixin dimer	-150.29

Photoelectric response of sensitized solar cells with natural dyes

The photocurrent - voltage plots of DSSC devices are shown in Figure 16. The parameters of DSSCs sensitized with natural dyes measured under AM 1.5 solar light (1000 W m^{-2}), are summarized in Table 2. The results show that the best power conversion efficiency (PCE) was achieved by cell manufactured with *Bixa orellana* extract due to the higher short-circuit current density (j_{SC}) in comparison with *Zea mays* sensitized solar cell.

Table 2. *Characteristic parameters of cells manufactured with Zea mays and Bixa orellana*

Cell	j_{SC} / mA cm^{-2}	V_{OC} / V	FF	η / %
Zea mays (C3G)	0.889 ± 0.032	0.590 ± 0.006	0.580 ± 0.057	0.304 ± 0.004
Bixa orellana (Bixin)	1.263 ± 0.106	0.610 ± 0.049	0.599 ± 0.026	0.462 ± 0.025

Table 3 shows the characteristic parameters of solar cells manufactured with other natural products based on anthocyanins and carotenoids. It is observed that the cells manufactured with *Zea mays* and *Bixa orellana* present better efficiencies than the other previously reported dyes.

Table 3. *Characteristic parameters of cells manufactured with other natural products containing anthocyanin and carotenoid*

Plant source	Structural class	j_{SC} / mA cm^{-2}	V_{OC} / V	FF	PCE, %	Reference
Rosa Xanthina	Anthocyanin	0.637	0.492	0.52	na	[40]
Tradescantia Zebrina	Anthocyanin	0.630	0.350	0.55	0.23	[47]
Begonia	Anthocyanin	0.630	0.537	0.72	0.24	[48]
Ixora macrothyrsa	Anthocyanin	1.310	0.400	0.57	0.30	[6]
Capsicum	Carotenoid	0.225	0.412	0.63	n.a.	[40]
Gardenia Blue	Carotenoid	0.530	0.440	0.69	0.16	[49]
Allamanda cathartic	Carotenoid	0.878	0.405	0.54	0.40	[50]

n.a. - not applicable

Figure 17 shows the incident-photon-to-current conversion efficiencies (IPCE) spectra obtained with the natural dyes. The IPCE corresponds to the number of electrons, measured as photocurrent in the external circuit, divided by the monochromatic photon flux that strikes the cell. The results are in good agreement with the short-circuit current (j_{SC}) values obtained from the current density-voltage (j - V) curves. Further, the maximum peaks of the IPCE, 6.58 % at 530 nm for *Zea mays* and 12.42 % at 510 nm for *Bixa orellana*, are located within the corresponding regions of maximum absorption observed in Figures 7 and 8.

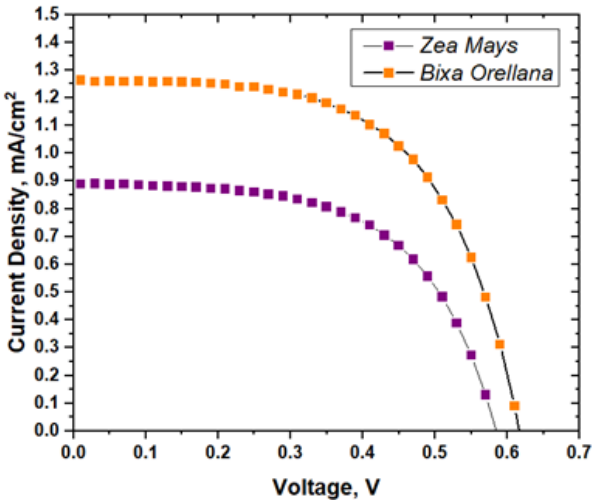

Figure 16. *Curves of current density as a function of voltage for cells manufactured with natural dyes*

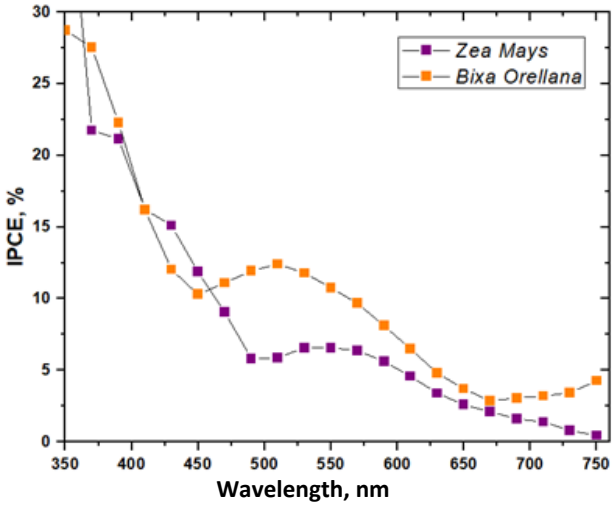

Figure 17. *Incident-photon-to-current conversion efficiencies (IPCE) absorption spectra of DSSC utilizing dye extracted from purple corn and achiote*

Discussion

The evidence of interaction between dye molecules and TiO_2 found in optical characterizations were confirmed with the final results of MDS in the following aspects. In the case of C3G, the deprotonation of the OH group and the formation of hydrogen bonds promote the chemisorption event, and create the close inter molecule interaction corresponding to -H bonds as observed in IR spectra. Intra molecular -H bond was observed in the repeated interaction between the C2'glycoside and C3' hydroxyl by means of proton exchange in MDS. The C-H of the glycosidic part forms a hydrogen bond, while that of the benzene ring weakens after the torsion in C5'. All these interactions cause the C-H bond to become less energetic, obtaining a red shift. Evidence of Ti-O bonding was found in IR and UV-Visible spectra. According to the structure of C3G, the ideal anchor with TiO_2 would be through the two hydroxyl groups of the molecule benzene-diol [40], following the bidentate mechanism of typical ruthenium-based molecules [51]. However, MDS confirm a bond through hydroxyl groups of C4' and disregard that it can occur through the other branches of cyanidin. This agrees with the optimized structures of anthocyanin-TiO_2 adsorption complexes of Marcano [52] that were also formed with a monodentate bond.

In the case of bixin, the peaks in IR and UV-Visible spectra of sensitized films showed a strong tendency to agglomeration. This was corroborated with the highest binding energies calculated for the bixin dimers. Although both dyes have a high affinity to form aggregates, the optimized structures of the bixin dimer are organized in such a way that generate π-π interactions between its chains. This type of aggregation in carotenoids was previously observed by Tay-Agbozo *et al*.[53], and it is stronger than Van der Waals bonds present in C3G dimer. The evidence of Ti-O bonding was also found in the IR spectrum, and it was confirmed by MDS that it occurs through the carboxylic group. MDS also shows a greater affinity to the point of completely folding over the cluster of TiO_2. In this configuration, hydrogen bonds could be observed in the $-CH_3$ groups that caused the red shift in the corresponding peak in IR spectrum.

The broadening of UV-vis absorbance spectra of dyes after sensitization is the experimental evidence of electronic transfer through the formed Ti-O bonds. The passivation of TiO_2 surface due to the loss of protons from the molecules is a point in favor since through hydrogenization the photocatalytic activity of TiO_2 can be improved to provide more free electrons [54]. In this sense, it is possible than greater affinity of bixin leads to having a large number of molecules available for electron transfer and to a greater passivation. However, the formation of aggregates on the surface of TiO_2 implies the appearance of intermolecular processes which decrease the efficiency of electron injection from excited states [55]. Despite this, the photocurrent obtained by the cell manufactured with *Bixa orellana* (1.263 mA cm^{-2}) was higher than that obtained with *Zea mays* (0.889 mA/cm^2). Likewise, the incident photon to current conversion efficiency was also higher in the case of *Bixa orellana*. Therefore, we can affirm that the conduction of free electrons through the film sensitized with bixin is more efficient compared to C3G.

The electronic transport through the film sensitized with *Zea mays* and *Bixa orellana* into the solar cell system was previously studied in detail by Huamán *et al*. [56]. The work concluded that better photocurrent achieved by the *Bixa orellana*, despite its the tendency to aggregation, can be explained by a higher resistance to recombination in the sensitized film. Recombination in solar cells is explained by the presence of a trap state distribution due to the surface modification. In energy terms, a higher density of trap states implies a lower Fermi level of the film [57]. The greater distribution of C3G trap states is reflected in the lower V_{OC} obtained from the characteristic *j*-V curves. To avoid a decrease in the Fermi level of the film, the effect of passivation during

chemisorption must be controlled and this can be achieved with an increase of pH. In their work on optimizing dye-sensitized solar cells with anthocyanins Chien *et al*. [58] found that efficiency increased with pH. Indeed, low pH can suppress deprotonation causing poor anthocyanin binding. This would lead to a low injection of electrons in the TiO_2 conduction band and increase the probability of charge recombination.

H-aggregation models at the TiO_2/dye interface, where blue-shifted absorption spectra are observed, have been widely reported in the literature [59-62]. However, the intermolecular interaction of bixin aggregates with TiO_2 surface has not yet been modeled. For now, our results show that this type of aggregation is present and is an important factor that limits the efficiency of the solar cell. Marotta *et al*. studied the effect of aggregation of dye D5 [61]. This molecule, like bixin, has a central chain and a carboxylic branch for bonding with TiO_2, and their maximum absorption peaks are remarkably close. They found that pretreatment with hydrochloric acid on the TiO_2 film induces the stabilization of charge transfer from the excited state and attenuates intermolecular interactions. In this sense, it is highly recommended to carry out this treatment before the bixin chemisorption process, in order to mitigate the aggregation effects and achieve better efficiencies.

Conclusions

Molecular dynamic simulation provided important information about the sensitization mechanisms of TiO_2 by natural dyes, which were validated by UV-Visible and FT-IR characterizations. The results indicated that the sensitization of C3G was a monodentate anchor through C4' hydroxyl groups of the benzene-diol of the molecule. The interaction caused hydrogen bonds and the passivation of TiO_2 with protons from the glycoside part of the molecule. On the other hand, bixin showed greater affinity with TiO_2 folding over it and forming a bond through the carboxylic group of the molecule. Bixin also showed a tendency to dimer formation due to π-π interactions between molecules, facilitating the aggregation on the surface, what was verified by the optical characterizations.

The events analyzed during the interaction of dyes and TiO_2 allow a better overview of the sensitized films through which the current is produced in the solar cell. The affinity of bixin with the surface of TiO_2 allows the more effective formation of Ti-O bonds and thus generates free electrons for conduction. Detrimentally, however, aggregation causes less efficient injection of electrons. C3G does not have a strong tendency to aggregate but presents a higher trap states density for free electrons, increasing the charge recombination and decreasing the generated photocurrent. Therefore, in order to obtain better efficiencies in the future, we recommend carrying out a study of the effects of pH in TiO_2 sensitization process with the colorant extracted from *Zea mays*, while in the case of *Bixa orellana*, the treatment of TiO_2 film with hydrochloric acid could be recommended. In sum, the state of the TiO_2 surface is a critical factor for adequate chemisorption of each particular dye, therefore new models of TiO_2 clusters with different levels of protonation must be considered for the analysis of the interaction with aggregates of these natural dyes.

***Acknowledgements**: The authors gratefully acknowledge support from the PhD program in Physics of the National University of Engineering funded through Resolution No. 168-2015- FONDECYT and the equipment project financed through Resolution No. 008-2018-FONDECYT-BM.*

References

[1] M. Grätzel, *Journal of Photochemistry and Photobiology C: Photochemistry Reviews* **4(2)** (2003) 145-153. https://doi.org/10.1016/S1389-5567(03)00026-1

[2] S. Aghazada, P. Gao, A. Yella, G. Marotta, T. Moehl, J. Teuscher, J. E. Moser, F. De Angelis, M. Grätzel, M. K. Nazeeruddin, *Inorganic Chemistry* **55(13)** (2016) 6653-6659. https://doi.org/10.1021/acs.inorgchem.6b00842
[3] M. Ye, X. Wen, M. Wang, J. Iocozzia, N. Zhang, C. Lin, Z. Lin, *Materials Today* **18(3)** (2015) 155-162. https://doi.org/10.1016/j.mattod.2014.09.001
[4] T. S. Senthil, N. Muthukumarasamy, D. Velauthapillai, S. Agilan, M. Thambidurai, R. Balasundaraprabhu, *Renewable Energy* **36(9)** (2011) 2484-2488. https://doi.org/10.1016/j.renene.2011.01.031
[5] K. Galappaththi, A. Lim, P. Ekanayake, M. I. Petra, *International Journal of Photoenergy* (2017). https://doi.org/10.1155/2017/8564293
[6] K. Wongcharee, V. Meeyoo, S. Chavadej, *Solar Energy Materials and Solar Cells* **91(7)** (2007) 566-571. https://doi.org/10.1016/j.solmat.2006.11.005
[7] S. A. Mozaffari, M. Saeidi, R. Rahmanian, *Spectrochimica Acta Part A: Molecular and Biomolecular Spectroscopy* **142** (2015) 226-231. https://doi.org/10.1016/j.saa.2015.02.003
[8] S. Dayang, M. Irwanto, N. Gomesh, *Indonesian Journal of Electrical Engineering and Computer Science* **9(1)** (2018) 191-197. https://doi.org/10.11591/ijeecs.v9.i1.pp191-197
[9] P. Chaiamornnugool, S. Tontapha, R. Phatchana, N. Ratchapolthavisin, S. Kanokmedhakul, W. Sang-aroon, V. Amornkitbamrung, *Journal of Molecular Structure* **1127(5)** (2017) 145-155. https://doi.org/10.1016/j.molstruc.2016.07.086
[10] D. Eli, M. Yusuf Onimisi, S. Garba Abdu, E. Jonathan, M. Y. Onimisi, S. G. Abdu, S. O. Yakubu, J. Miguel Dias, *British Journal of Applied Science & Technology* **15(2)** (2016) 1-6. https://doi.org/10.9734/BJAST/2016/24437
[11] Y. Kimura, T. Maeda, S. Iuchi, N. Koga, Y. Murata, A. Wakamiya, K. Yoshida, *Journal of Photochemistry and Photobiology A: Chemistry* **335** (2017) 230-238. https://doi.org/10.1016/j.jphotochem.2016.12.005
[12] N. Prabavathy, S. Shalini, R. Balasundaraprabhu, D. Velauthapillai, S. Prasanna, P. Walke, N. Muthukumarasamy, *Journal of Materials Science: Materials in Electronics* **28** (2017) 9882-9892. https://doi.org/10.1007/s10854-017-6743-7
[13] A. S. Najm, A. B. Mohamad, N.A. Ludin, *AIP Conference Proceeding* **1838** (2017). https://doi.org/10.1063/1.4982191
[14] M. A. M. Al-Alwani, A. B. Mohamad, A. A. H. Kadhum, N. A. Ludin, *Spectrochimica Acta Part A: Molecular and Biomolecular Spectroscopy* **138** (2015) 130-137. https://doi.org/10.1016/j.saa.2014.11.018
[15] K. U. Isah, U. Ahmadu, A. Idris, M. I. Kimpa, U. E. Uno, M. M. Ndamitso, N. Alu, *Materials for Renewable and Sustainable Energy* **4** (2015) 39. https://doi.org/10.1007/s40243-014-0039-0
[16] C. I. Oprea, A. Dumbrava, I. Enache, A. Georgescu, M. A. Gîrţu, *Journal of Photochemistry and Photobiology A: Chemistry* **240** (2012) 5-13. https://doi.org/10.1016/j.jphotochem.2012.05.003
[17] A. R. Pai, B. Nair, *Bulletin of Materials Science* **38** (2015) 1129-1133. https://doi.org/10.1007/s12034-015-0991-z
[18] R. Syafinar, N. Gomesh, M. Irwanto, M. Fareq, Y. M. Irwan, *Energy Procedia* **79** (2015) 896-902. https://doi.org/10.1016/j.egypro.2015.11.584
[19] M. A. M. Al-Alwani, A. B. Mohamad, A. Amir, H. Kadhum, N. A. Ludin, *Asian Journal of Chemistry* **26(18)** (2014) 6285-6288. https://doi.org/10.14233/ajchem.2014.17742
[20] S. Z. Siddick, C. W. Lai, J. C. Juan, *Materials Science in Semiconductor Processing* **74** (2018) 267-276. https://doi.org/10.1016/j.mssp.2017.10.046
[21] M. Rossi, F. Matteocci, A. Di Carlo, C. Forni, *Journal of Plant Science and Phytopathology* **1** (2017) 087-094. https://doi.org/10.29328/journal.jpsp.1001011
[22] E. Yamazaki, M. Murayama, N. Nishikawa, N. Hashimoto, M. Shoyama, O. Kurita, *Solar*

Energy **81(4)** (2007) 512-516. https://doi.org/10.1016/j.solener.2006.08.003
[23] K. V Hemalatha, S. N. Karthick, C. J. Raj, N. Hong, S. Kim, H. Kim, *Spectrochimica Acta Part A: Molecular and Biomolecular Spectroscopy* **96** (2012) 305-309. https://doi.org/10.1016/j.saa.2012.05.027
[24] H. Hug, M. Bader, P. Mair, T. Glatzel, *Applied Energy* **115** (2014) 216-225. https://doi.org/10.1016/j.apenergy.2013.10.055
[25] S. De Pascual-Teresa, C. Santos-Buelga, J. C. Rivas-Gonzalo, *Journal of the Science of Food and Agriculture* **82** (2002) 1003-1006. https://doi.org/10.1002/jsfa.1143
[26] P. Sahni, *Advanced Science Letters* **5(1)** (2012) 1-10. https://doi.org/10.1166/asl.2012.1961
[27] A. K. Pandey, M. S. Ahmad, N. A. Rahim, V. V. Tyagi, R. Saidur, *Environmental Biotechnology: For Sustainable Future* (2019) 375-401. https://doi.org/10.1007/978-981-10-7284-0_15
[28] R. E. Wrolstad, R. W. Durst, J. Lee, *Trends in Food Science & Technology* **16(9)** (2005) 423-428. https://doi.org/https://doi.org/10.1016/j.tifs.2005.03.019
[29] T. Taham, F. A. Cabral, M. A. S. Barrozo, The *Journal of Supercritcal Fluids* **100** (2015) 175-183. https://doi.org/https://doi.org/10.1016/j.supflu.2015.02.006
[30] N. T. R. N. Kumara, P. Ekanayake, A. Lim, L. Y. C. Liew, M. Iskandar, L. C. Ming, G. K. R. Senadeera, *Journal of Alloys and Compounds* **581** (2013) 186-191. https://doi.org/10.1016/j.jallcom.2013.07.039
[31] Y. Han, D. Jiang, J. Zhang, W. Li, Z. Gan, J. Gu, *Frontiers of Chemical Science and Engineering* **10** (2016) 16-38. https://doi.org/10.1007/s11705-015-1545-z
[32] E. Güzel, B. S. Arslan, V. Durmaz, M. Cesur, Ö. F. Tutar, T. Sarı, M. İşleyen, M. Nebioğlu, İ. Şişman, *Solar Energy* **173** (2018) 34-41. https://doi.org/10.1016/j.solener.2018.07.048
[33] Y. Ooyama, M. Kanda, T. EnoKi, Y. Adachi, J. Ohshita, *RSC Advances* **7(22)** (2017) 13072-13081. https://doi.org/10.1039/C7RA00799J
[34] L. Daniliuc, C. De Kesel, C. David, *European Polymer Journal* **28(11)** (1992) 1365-1371. https://doi.org/10.1016/0014-3057(92)90277-9
[35] A. H. Ahliha, F. Nurosyid, A. Supriyanto, T. Kusumaningsih, *IOP Conference Series: Materials Science and Engineering* **333** (2018) 12018. https://doi.org/10.1088/1757-899x/333/1/012018
[36] T. Lóránd, P. Molnár, J. Deli, G. Tóth, *Journal of Biochemical and Biophysical Methods* **55(1-3)** (2002) 251-258. https://doi.org/10.1016/S0165-022X(02)00113-6
[37] Y. Ooyama, S. Inoue, T. Nagano, K. Kushimoto, J. Ohshita, I. Imae, K. Komaguchi, Y. Harima, *Angewandte Chemie International Edition* **50** (2011) 7429-7433. https://doi.org/10.1002/anie.201102552
[38] C. Bonechi, S. Martini, A. Magnani, C. Rossi, *Magnetic Resonance in Chemistry* **46(7)** (2008) 625-629. https://doi.org/https://doi.org/10.1002/mrc.2217
[39] Q. Dai, J. Rabani, *Journal of Photochemistry and Photobiology A: Chemistry* **148(1-3)** (2002) 17-24. https://doi.org/10.1016/S1010-6030(02)00073-4
[40] S. Hao, J. Wu, Y. Huang, J. Lin, *Solar Energy* **80(2)** (2006) 209-214. https://doi.org/10.1016/j.solener.2005.05.009
[41] G. Calogero, G. Di Marco, *Solar Energy Materials and Solar Cells* **92(11)** (2008) 1341-1346. https://doi.org/10.1016/j.solmat.2008.05.007
[42] K. Vinodgopal, X. Hua, R. L. Dahlgren, A. G. Lappin, L. K. Patterson, P. V. Kamat, The *Journal of Physical Chemistry* **99(27)** (1995) 10883-10889. https://doi.org/10.1021/j100027a032
[43] M. A. Montenegro, A. D. O. Rios, A. Z. Mercadante, M. A. Nazareno, C. D. Borsarelli, *Journal of Agricultural and Food Chemistry* **52(2)** (2004) 367-373. https://doi.org/10.1021/jf0349026
[44] T. Ma, K. Inoue, H. Noma, K. Yao, E. Abe, *Journal of Photochemistry and Photobiology A: Chemistry* **152(1-3)** (2002) 207-202. https://doi.org/10.1016/S1010-6030(02)00025-4

[45] A. Ehret, L. Stuhl, M. T. Spitler, *Electrochimica Acta* **45(28)** (2000) 4553-4557. https://doi.org/10.1016/S0013-4686(00)00606-X
[46] L. Zhang, J. M. Cole, *ACS Applied Materials & Interfaces* **7(6)** (2015) 3427-3455. https://doi.org/10.1021/am507334m
[47] P. G. Bomben, K. D. Thériault, C. P. Berlinguette, *European Journal of Inorganic Chemistry* **2011(11)** (2011) 1806-1814. https://doi.org/10.1002/ejic.201001345
[48] E. Marcano, *Energy Harvesting and Systems* **5(1-2)** (2018) 29-38. https://doi.org/10.1515/ehs-2018-0008
[49] S. Tay-Agbozo, S. Street, L. D. Kispert, *Journal of Photochemistry and Photobioly A: Chemistry* **362** (2018) 31-39. https://doi.org/10.1016/j.jphotochem.2018.05.008
[50] X. Chen, L. Liu, P. Y. Yu, S. S. Mao, *Science* **331(6018)** (2011) 746-750. https://doi.org/10.1126/science.1200448
[51] H. Ozawa, M. Awa, T. Ono, H. Arakawa, *Chemistry - An Asian Journal* **7(1)** (2012) 156-162. https://doi.org/10.1002/asia.201100484
[52] A. A. Huamán, M. R. Celestino, M. E. Quintana, *RSC Advances* **11** (2021) 9086-9097. https://doi.org/10.1039/D1RA01043C
[53] F. Cao, G. Oskam, G. J. Meyer, P. C. Searson, *The Journal of Physical Chemistry* **100(42)** (2002) 17021-17027. https://doi.org/10.1021/jp9616573
[54] C. Y. Chien, B. D. Hsu, *Solar Energy* **98(C)** (2013) 203-211. https://doi.org/10.1016/j.solener.2013.09.035
[55] A. El-Zohry, A. Orthaber, B. Zietz, *The Journal of Physical Chemistry C* **116(50)** (2012) 26144-26153. https://doi.org/10.1021/jp306636w
[56] S. Agrawal, T. Leijtens, E. Ronca, M. Pastore, H. Snaith, F. De Angelis, *Journal of Materials Chemistry A* **1(46)** (2013) 14675-14685. https://doi.org/10.1039/C3TA12917A
[57] G. Marotta, M. G. Lobello, C. Anselmi, G. Barozzino Consiglio, M. Calamante, A. Mordini, M. Pastore, F. De Angelis, *ChemPhysChem* **15(6)** (2014) 1116-1125. https://doi.org/10.1002/cphc.201300923
[58] L. Zhang, X. Liu, W. Rao, J. Li, *Scientific Reports* **6** (2016) 35893. https://doi.org/10.1038/srep35893